View metadata, citation and similar papers at core.ac.uk

brought to you by CORE

provided by NASA Technical Reports Server

CR 114537

NAS5-9311

Plasma Measurements with the Retarding Potential Analyser on OGO VI

by

W. B. Hanson, S. Sanatani, D. Zuccaro, and T. W. Flowerday**

The University of Texas at Dallas*
P. O. Box 30365
Dallas, Texas 75230

CASE FILE COPY

June 1970

Accepted for Publication by

Journal of Geophysical Research

**Now at Atlantic Research Corporation, Costa Mesa, California
*Formerly Southwest Center for Advanced Studies

SP-70-016

Abstract

The nature of the results from the retarding potential analyser on OGO VI are described. The device appears capable of measuring ion temperature to an accuracy of better than ten percent in a quiet ionosphere. In the dawn-dusk plane the ion temperature is observed to vary from 1000°K to 4000°K; the higher temperatures being associated with higher altitudes in the winter hemisphere. Molecular ions are detected near perigee (400 km), but their concentrations seldom exceed one percent of the O^+ ion concentration. At mid-latitudes and higher altitudes (>700 km) the lighter ions H^+ and He^+ are both present at approximately the O^+ concentration but their relative importance decreases near and in the polar regions. Both polar regions display large spatial fluctuations in ion concentration and this behavior extends somewhat into the plasmasphere. Fluxes of electrons with energy greater than 10 ev of the order of 10^8 cm^{-2} sec^{-1} are observed that change rather smoothly within the plasmasphere but show rapid and large variations at higher latitudes. The device also operates in a mode that examines the horizontal changes in ion concentration (fractional changes as small as 10^{-3} can be observed) with a spatial resolution from 350 meters to as small as 40 meters, depending on the telemetry rate.

Introduction

A planar geometry retarding potential analyser (RPA), commonly called an ion trap, was included in the payload of OGO VI. Because the OGO's are oriented vehicles they provide ideal platforms for the operation of planar ion traps. OGO VI was launched into a dawn-dusk orbit on June 5, 1969, from the Western Test Range at 1440 GMT and the initial orbital parameters were perigee 397 km, apogee 1098 km, and inclination 82°. The purpose of this report is to describe the operation of the RPA and the nature of the data obtained. In general, the initial results are very promising and it appears that accurate and reliable values for ion temperature and concentration can be derived.

Many previous attempts have been made to measure ion temperature with planar and spherical RPA's in both rockets and satellites, with varying degrees of success. The first reported measurements with an RPA came from the spherical ion trap in Sputnik 3 (Krassovsky, 1959), but the behavior of devices with spherical geometry is sufficiently different (from those with planar geometry) that their performance will not be reviewed.

The first reported measurements of ion temperature with a planar RPA in a rocket were by Hanson and McKibbin (1961), but they felt the values of T_i deduced from their measurements (1900°K to 2800°K) were too high to be valid. Subsequent rocket results by Knudsen and Sharp (1965) in the E layer revealed considerable vertical structure in T_i.

Knudsen and Sharp (1966) also reported some measurements of T_i in a rocket of unknown orientation above 700 km, where it was assumed that H^+ was the dominant ion. Quite reasonable values of ion temperatures were deduced ($\sim$1200°K). Hanson et al. (1969) measured T_i in the 300 km to 700 km altitude range and argued that the values obtained were in reasonable agreement with theory. All the above measurements showed considerable scatter in the deduced values of T_i, and all data analyses were performed using only the most appropriate of the several linear voltage output ranges available.

The high mach number available in satellites, as well as the long time available for outgassing, makes them appear more inviting than rockets as an RPA platform. Hanson et al. (1964) and Knudsen and Sharp (1967) presented the first T_i results from a satellite RPA. The altitude range 210 km to 516 km was examined. Ion temperatures varied from approximately 1000°K to more than 5000°K, with considerable scatter in the data. Again, only one of three linear voltage ranges was used to deduce a given value of T_i, so that a large dynamic range in ion current was not available. A rather noisy telemeter system also tended to degrade the accuracy of the data. Harris et al. (1967, 1969) measured T_i on another low altitude satellite in the height range of approximately 130 km to 300 km. Data analysis on the ground was again restricted to a single linear voltage scale on a relatively noisy telemeter. This limitation was partially overcome, however, with the aid of on-board data processing, and while the reported T_i values show

much horizontal structure, there was relatively little scatter in the data. The magnitude of T_i varied from less than 400°K to greater than 4000°K, so that it appears most unlikely that T_i is even approximately equal to the neutral particle temperature, T_n, if these results are valid. While it is relatively easy to hypothesize effects that would make $T_i > T_n$, it is somewhat disturbing that T_i was observed to be lower than 400°K on occasion at altitudes well above 200 km. Radar backscatter results at Jicamarca for the same time interval gave minimum values of T_i of approximately 650°K above 200 km (McClure, 1969).

Recently Donley (1969) and Donley et al. (1969) presented some preliminary data from the planar RPA on Explorer XXXI, which had an initial perigee and apogee of 502 km and 2982 km respectively. The rather low maximum retarding potential used (6.3 volts) precludes the possibility of examining the high energy Boltzman tail of the O^+ ion distribution, but this should be possible for the light ions H^+ and He^+. While the limited data presented appeared to be reasonable, the T_i results were consistently higher (by from 20% up to a factor of two) than obtained with a spherical ion probe (Wrenn, 1969; Donley et al., 1969) on the same satellite. The raw data from the spherical probe (Wrenn, 1969) taken near perigee are quite impressive and appear to be of much better quality than that obtained with a similar instrument on Ariel I (Boyd and Raitt, 1965; Bowen et al., 1964).

The following presentation describes first the physical nature and operating characteristics of the RPA on OGO VI. Next the form of the raw data and the technique of data analysis are shown and discussed.

A relatively small amount of reduced data is then given, which is meant more to illustrate the kind of results obtained than to examine their physical significance. It is expected that the correlation of the RPA measurements with other geophysical parameters being simultaneously monitored on OGO VI will be much more fruitful than considering these results alone. Such joint efforts await the issuance of final format data tapes from the OGO data processing center and analysis of the data by the individual experimenters. A rather extensive discussion of the limitations of the data is indulged so that the validity of future results as well as those presented here can be adequately judged by the reader.

Description of the experiment

The Retarding Potential Analyser (RPA) is comprised of a sensor head and a contiguously mounted electronics box which together weigh 2.75 lbs. and consume 1.8 watts of power.

The sensor head consists of an 8 cm diameter cylinder with a 2 cm diameter aperture through which charged particles pass before striking a solid collector. The path between the aperture and collector is electrically segmented by a series of grids whose potentials are controlled by the electronics box, (see figure 1). The grids are all made of 100 mesh (i.e., two perpendicular sets of wires 10 mils apart) gold plated 1 mil tungsten wire, and all other metal surfaces in the sensor head are also gold plated.

The sensor head is flush mounted on the orbital plane experimental package (OPEP) number 1, which is always on the earth side of the main body. Surrounding the sensor head is a grounded gold plated 16 mesh screen that is fared out a distance 6.5 mm ahead of the sensor face, as shown in Figure 1. This screen, whose purpose is to minimize electric fields parallel to the sensor face, covers the entire OPEP front surface, except for instrument apertures, and is also wrapped over the edges of the OPEP for several centimeters. The edge closest to the sensor face is 3 centimeters away. During normal operation the sensor face is perpendicular to the vehicle velocity vector.

The electronics box contains a power supply with several fixed output voltages, an automatic range-changing linear electrometer, a differential amplifier and a linear voltage sweep circuit, together with several logic and timing networks. The electrometer has a sensitivity of 3.02×10^{-11} amperes per volt on the most sensitive of 8 different amplification ranges and responds equally to positive and negative currents. Adjacent ranges have voltage gains that differ by a factor of $\sqrt{10}$. The difference amplifier has a gain of 50.

Modes of Operation:

There are two basic modes of operation. During the ion-analysis mode, when the ion temperature and composition are examined, the retarding grid, G_3, is swept linearly from +19.5 volts to -1.8 volts and three of the four main frame telemetry words allotted to this experiment are assigned to the electrometer output. During the duct-mode, when small horizontal gradients in ion concentration are examined, grid G_3 is maintained at -1.8 volts and three of the four telemetry words

are assigned to the differential amplifier output while the fourth reads the electrometer output. Grid G_4 (the suppressor grid) is always maintained at -9.1 volts (all voltages given are with respect to vehicle ground) to suppress photoemission from the collector and grids G_1 and G_2 are always grounded.

The differential amplifier monitors the difference between the electrometer output voltage at the time the duct mode is initiated and its subsequent voltage output. This difference voltage is amplified by a factor of 50 and presented to the telemeter. Zero output of the differential amplifier is set at 2.68 volts on the telemetry output so that both plus and minus changes in the electrometer output can be observed. The polarity of the differential amplifier is such that an increase in its voltage output corresponds to a decrease in the electrometer voltage output.

The two modes are alternately employed and approximately equal time is devoted to each one. A complete cycle time of either 40 seconds or 10 seconds can be selected by ground command, except that during real time readout, when a higher data rate is employed, the 10 second period is automatically invoked.

Telemetry:

Four main frame telemetry words are assigned to the instrument. Each of these words is tape recorded in digital form with 8 bit accuracy every 0.144 seconds during the 8 kbit storage mode. During real time interrogation, when the tape recorder is not being read out, the data

may be taken in real time at 16 kbit, 32 kbit, or 64 kbit rates, with a proportionately smaller time interval between word transmissions. The sweep voltage and electrometer sensitivity range were monitored on a subcommutator at much lower data rates.

Data Analysis

A sample of the raw-data returned is illustrated in Figure 2, where a complete cycle of both modes is shown. The data was tape recorded at the 8 kbit rate. The upper trace is made by the single word which continuously monitors the electrometer output. The middle trace is made by the two switched words which alternately monitor the electrometer output and the difference amplifier output. The lowest trace is a reconstructed voltage sweep of the potential applied to grid G_3 based on the subcommutator voltage information. The fourth main frame word, which continuously monitors the differential amplifier output, is not shown.

When the retarding potential is large and positive (point A) the electrometer reads the current due to fast electrons entering the sensor aperture that can overcome the -9.1 volt potential on grid G_4. (They must also have sufficient energy to overcome the negative potential of the OPEP with respect to the ambient plasma.) There is a short recovery time before point A where the electrometer recovers from the previous mode switching operation. As the positive retarding potential decreases, the more energetic ions (in the vehicle frame of reference)

begin to reach the collector (point B) and the net current decreases towards zero where the electrometer polarity is automatically switched. The ion current then continues to increase till the electrometer output reaches +4.5 volts at which time the electrometer sensitivity is automatically reduced by a factor of approximately $\sqrt{10}$. The electrometer sensitivity is changed four more times in this manner until the ion current saturates, i.e. until all ions entering the sensor aperture are being collected.

At point C the instrument changes to the duct mode, where the switched words begin to monitor the difference amplifier output. The duct mode continues to point D, where the cycle ends and the ion analysis mode is repeated again.

Duct Mode:

In the duct mode, small changes in the electrometer output can be observed on the differential amplifier output. If the electrometer voltage at the beginning of the duct mode is denoted by V_o and the difference amplifier output by V_d, the percentage change in the electrometer current, δ, is given by

$$\delta = -2 \frac{(V_d - 2.6)}{V_o} \qquad (1)$$

Since the satellite velocity changes very slowly with time, δ may be considered to be proportional to changes in the ambient ion concentration provided that other parameters (i.e. angle of attack) also do not change rapidly. The fact that V_o is seldom less than 1.5 volts means that changes in n_i larger than ± 3.5 percent cannot be observed with the

differential amplifier. Changes larger than this can be readily observed directly on the electrometer output but with only one third the time resolution provided by the differential amplifier output. The ultimate sensitivity of the duct mode occurs when V_o = 4.5 volts. Under these conditions a one bit change (20 mv) in V_d corresponds to a change of approximately 0.01 percent in n_i.

Some representative examples of the difference amplifier output taken at the 64 kbit rate during real time telemetry readout are displayed in Figure 3. The upper trace (a) shows a very uniform gradient in n_i of +0.083 percent per kilometer. On many occasions such uniform gradients are observed, often properly identified with increasing or decreasing height of the satellite, but many times with an unexpected algebraic sign, which can only indicate real horizontal gradients in n_i. The second trace (b) shows small periodic changes in n_i about a constant mean value with a wavelength of 4 km. The amplitude of the sinusoidal changes is less than 0.1 percent. Such an event is relatively rare but the trace is by no means unique. Quite often the traces are flat over the entire trace to less than 0.05 percent. The lower trace (c) shows considerable fine structure with varying amplitude and period. Traces similar to this are observed on every orbit examined, together with many of even larger amplitude. Individual points are recorded every 40 meters along the orbital path during this 64 kbit real time readout, and it is obvious that the structure extends to horizontal distances much smaller than a kilometer. Observation of such fine structure at larger amplitudes (δ>5%) has been previously reported by Dyson (1969).

Ion Analysis Mode:

The ion currents shown in Figure 2 are replotted in Figure 4 on a semilog plot of collector current versus retarding potential; only every fourth data point has been plotted. The smallest ion currents, which contain relatively large bit-error, are not shown (one bit on range 1 corresponds to a current of approximately 6×10^{-13} amperes) but even so the data extend over 3 1/2 decades of collector current. Current-voltage characteristic curves, as illustrated in Figure 4, are fitted by a least squares technique (Patterson, 1969) to the theoretical expression (Whipple, 1959):

$$J = \frac{1}{2} K V A \varepsilon \sum_i n_i \left[1 + \text{erf}\ (\beta_i f_i) + \frac{1}{\sqrt{\pi}\ \beta_i V} \exp\ (-\beta_i^2 f_i^2)\right] \qquad (2)$$

where

J = collector current

K = grid transmission factor

n_i = concentration of i^{th} ion

$V = v \cos \theta$

v = magnitude of vehicle velocity vector in the plasma frame of reference

θ = angle of attack

A = area of aperture

$f_i = V - [2 \varepsilon (U + \psi)/m_i]^{1/2}$

ε = ionic charge

$\beta_i = (m_i/2kT_i)^{1/2}$

m_i = mass of the i^{th} ion

T_i = ion temperature

k = Boltzmann constant

U = retarding grid potential with respect to vehicle ground

ψ = vehicle potential with respect to plasma

This curve fitting technique yields the optimum values for T_i, ψ, and the concentration of the various ion species present. The solid line shown represents the best fit of (2) to the data. The one obviously poor fitting point near $J = 5 \times 10^{-10}$ amps was recorded during a range change of the electrometer. It has been assumed in the present computer program that T_i is the same for all ion species, but this is not a necessary assumption. The quality of the fit of the theoretical expression to the data is expressed in terms of the root of the mean square fractional deviation, σ, i.e.,

$$\sigma = N^{-1/2}\left\{ \sum_{i=1}^{N} [(I_{calc} - I_{obs})/I_{obs}]_i^2 \right\}^{1/2} \qquad (3)$$

where N is the number of experimental points used in the analysis.

Analysis of the data in Figure 4 indicates that atomic oxygen is the principal ion present. At high positive retarding potentials the ion current is almost entirely due to heavier molecular ions, even though they amount to only a few tenths of a percent of the O^+ concentration. This is so because of the greater ram energy of the heavier ions in the vehicle frame of reference. At typical OGO velocities this ram energy is approximately 1/3 ev per AMU, so that molecular ions have approximately 4 or 5 ev more energy on the average

than the O^+ ions. Heavy ions are detected only at altitudes below approximately 600 km and their maximum fractional abundance, which occurs near perigee, is of the order of one percent.

The presence of light ions is evident at low retarding potentials in the data shown in Figure 5, where all the data, except that recorded near electrometer range changes, have been plotted. The least squares analysis indicates that the (He^+/H^+) and (He^+/O^+) concentration ratios are 3.6 and 2.2 respectively in this case. Because of the small ram energy of the light ions their appearance potential is low, and typically the O^+ current has already saturated before they produce a sensible current at the collector. Thus light ions cannot usually be detected at as small concentrations as the molecular ions because of the presence of these large background O^+ currents. Figures 4 and 5 exemplify rather extreme concentrations of molecular and light ions, respectively.

Results

Only a relatively small amount of data have been analysed to date, and most of that was taken shortly after launch when the vehicle was still in a dawn-dusk orbit. An example of a nearly-complete orbit of data is plotted versus magnetic latitude in Figure 6; altitude and geographic longitude are indicated at the top of the figure. The upper plot shows the behavior of the ion composition, which is dominated by O^+ ions over most of the path. The largest concentration is observed

near perigee, as might be expected. The ion concentrations are generally larger in the northern (summer) hemisphere, and a careful examination reveals that this is not entirely an altitude effect.

The asymmetry of the molecular ions about perigee is quite extreme; there is an order of magnitude more molecular ions at 450 km at high latitudes than at low latitudes, though the O^+ concentration is nearly the same. When the OGO VI data analysis is further along and comparisons with the neutral spectrometer aboard can be made it will be possible to tell whether this asymmetry is related to differences in the neutral atmospheric composition or to differences in the ionizing processes at these locations (or to some other effects).

On either side of the southern polar region the concentrations of H^+ and He^+ become important. Near 40°S latitude, O^+, H^+, and He^+ are all present in comparable, but rapidly changing, amounts. Poleward of this H^+ falls off rapidly, and He^+ somewhat more slowly. Whether this behavior is also present at great heights, and thus marks the plasmapause boundary, cannot be determined from this data alone. Over the south polar region (near apogee) the ionosphere becomes so structured that the curve fitting technique is no longer useful.

The second plot in Figure 6 shows how the ion temperature varies along the orbit. Perhaps the most striking feature is the high ion temperature in the southern (winter) hemisphere, particularly on the dusk side. T_i climbs steeply to 4000°K south of the magnetic equator, and this cannot be simply an altitude effect, though it does correlate with a rapid decrease in the total ion concentration. The minimum value of T_i occurs at low altitude near the dawn magnetic equator

crossing. The value of 1100°K is in reasonable agreement with the expected neutral gas temperature for this solar epoch. T_i appears to be approaching a secondary minimum near the southern polar region, but as stated above, it was not possible to analyze data in the highly structured region over the polar cap. This minimum in T_i at high southerly latitudes may reflect the fact that the solar zenith angle is a maximum here in the subsatellite ionosphere. Alternatively, it might be related to evaporative cooling by plasma that is escaping the ionosphere. At these latitudes a large plasma escape flux ($\sim 10^8$ $cm^{-2} sec^{-1}$) has been observed (Parks, 1969). Because the ion concentrations were larger in the northern polar region some of the data could be analyzed in spite of the structure with some sacrifice in accuracy; no large anomalies in T_i occurred. The dashed section shown in the Northern polar region represents the magnetic latitudes not covered on this orbit.

Values deduced for the vehicle potential are shown in the next plot. It is not expected that this quantity can be determined with great accuracy because of uncertainties in contact potential differences between the sensor head and the vehicle. Also, some of the scatter is due to the method of analysis, which did not fix the starting point of the retarding potential sweep with great accuracy because of the preliminary data format available. (The technique used did not compromise the voltage sweep rate, which is needed to determine T_i.) The values of ψ deduced fall in the range -1 to -4 volts, and are not unreasonable values.

The last plot in Figure 6 shows the variation in the fast electron fluxes observed. These values are obtained simply by dividing the

initial negative current (point A in Figure 2) by the effective aperture (AK) of the sensor. These currents could arise from atmospheric photoelectrons, secondary electrons, photo emission from the suppressor grid, or even by the release of photoelectrons from the skin of the vehicle (the latter seems rather unlikely for such high energy electrons). Their energy normal to the collector must exceed the suppressor grid potential (-9.1 volts) plus the vehicle potential unless they are released from the suppressor grid itself. Not all external electrons satisfying these conditions would be collected either because the collector subtends a solid angle from the aperture less than 2π. The effective solid angle depends on the energy of the electrons as well as the potential on the retarding grid. In spite of these uncertainties the magnitudes of the fluxes deduced ($\sim 10^{8}$ $cm^{-2} sec^{-1}$) appear to be in reasonable consonance with what might be expected for ambient photoelectrons.

The release of electrons from the suppressor grid structure by solar UV is a function of the angle between the sun and the normal to the trap face, and the magnitude of the resultant current can be determined experimentally. Some values for the photo emission current as a function of this angle were obtained on orbit 36 when the OPEP was scanning, and they are shown in Figure 7. Curiously, the current does not peak when the sun is normal to the trap face, but has two maxima, one near 45 degrees and one near 60 degrees. This behavior is probably due to the fact that the suppressor grid represents a rather

steep maximum in electron potential, which decreases rapidly towards both the collector and the retarding grid. At small solar angles nearly all the photo emission occurs on the retarding grid side of suppressor grid wires and relatively few of the electrons are able to reach the collector. At larger solar angles the underside of the suppressor grid wires become exposed and the resulting collector current increases to a secondary maximum and then decreases because the effective aperture area falls off rapidly at large solar angles. For solar angles greater than 51 degrees direct solar UV can reach the solid suppressor grid support ring and the emission current rises rapidly to its maximum value. The total angular width of this peak agrees quite well with the value 18° obtained from the sensor geometry shown in Figure 1.

The presence of even a large photo emission current does not seriously detract from the validity of the ion measurements, provided that this current does not change rapidly with time, because the ion currents are referenced to zero at the (constant) negative current present at large positive retarding potentials (see Figure 2).

The rather symmetric peak observed in Figure 6 in the electron flux near the dawn equator is usually present, though the width in latitude varies greatly. It may be caused by solar UV emission within the sensor head, but a final determination must await the complete satellite attitude information ultimately available. At higher latitudes, usually above 60° magnetic latitude, the nature of these negative currents changes abruptly. Large variations in magnitude can occur over very small distances, and the magnitude can be considerably larger

(or smaller) than observed at lower latitudes. We believe this change in character may be related to the edge of the energetic particle trapping zone or possibly to the plasmapause boundary.

Discussion of Errors

Determination of T_i:

On many occasions at middle and low latitudes a sequence of ten or more successive derived values of T_i will differ by less than one percent from a straight line drawn through the points (which may have zero slope). This is particularly true when the sequence time is ten seconds rather than forty seconds, so that the values are derived over a relatively small spatial domain. One such case is shown in Figure 8, where T_i is plotted versus latitude, and altitude is indicated at the top of the figure. Most of the data points shown deviate from the (arbitrary) straight line by less than 0.5% and all the points differ from their mean value by less than 1.5%. The missing points were eliminated before analysis because of obvious deficiencies due to telemeter dropout. The worst fitting point, near 6.5°, had a statistical deviation more than twice as large as any of the other points and could be ignored on this ground. The data were obtained at the lowest (8 kbit) information rate with a mode cycle period of ten seconds. Since the behavior of T_i depicted in Figure 8 is relatively common, it is obvious that the internal consistency of the method for deriving this parameter from the data is quite good and clearly no large random errors are present. In spite of this there are other

considerations that place larger limits on the absolute accuracy of the T_i determination.

In the absence of horizontal structure the fit of (2) to the data is generally quite satisfactory. The average percentage deviation of the points from the theoretical curve can be so small that it is difficult to obtain a feeling for the precision obtainable in the T_i parameter by inspection of a curve such as Figure 4. For this reason a plot of σ versus trial T_i values is shown in Figure 9 for the data shown in Figure 10. The least squares technique actually finds the best pairs of T_i and ψ values for a given value of one or the other and then seeks the minimum value of σ along this path. (The corresponding ψ values are also plotted.) It can be seen from the figure that a rather sharp minimum in σ exists near the best value of T_i; the "noise level" in σ is such that the resolution of better than one percent in T_i is readily obtainable in this quite typical instance. This conclusion is consistent with the data shown in Figure 8.

The deduced value of T_i depends on the retarding voltage sweep rate, dU/dt; hence any uncertainties in this slope will be reflected in an absolute uncertainty in the derived values of T_i. When the current for a single ion mass (i.e., O^+) is being analyzed the derived temperature depends on the square of dU/dt (Hanson, et al., 1964), so that the absolute uncertainty in T_i is twice as large as the uncertainty in dU/dt. This has been verified by using retarding potential slopes 5 percent larger and smaller than normal in the least squares program. The resulting values of T_i do indeed differ by 10

percent from the normal value, but the statistical fit is considerably worse in both cases. When more than one ion mass is present, it is found that the uncertainty in the derived values of T_i depends less drastically on the uncertainty in dU/dt. The voltage sweep rate was determined to within $\pm$ 1 percent prior to launch. Any systematic changes that occur in dU/dt subsequent to flight can be ascertained with great precision since U is monitored every sweep. Analysis of some of the flight data indicates that the sweep is indeed very linear, and the observed slope during the early flight phase agrees with the preflight value within experimental error.

In most cases the determination of T_i is based principally on the changes in the O^+ current as U is swept. It is assumed here that this current is due solely to O^+, though it is known from mass spectrometer measurements (Johnson, 1966) that up to 10 percent N^+ may be present. The consequences of this assumption on the derived values of T_i have been checked by generating theoretical collector-current versus U curves with different concentration ratios of N^+ to O^+ and then analyzing them assuming that only O^+ is present. The results are summarized in Table I. They indicate that the percentage error in the deduced value of T_i is approximately one tenth of the percentage of N^+ present. It is clear that the errors incurred in T_i as a result of the specific neglect of N^+ are small ($\leq$1%) unless unexpectedly large amounts of N^+ should occur. In any event, it is the sum of the actual N^+ and O^+ concentrations that we present as the O^+ concentration.

Table I

N^+/O^+	T_i(°K) Actual	T_i(°K) Calc.	ψ (volts) Actual	ψ (volts) Calc.
0.05	1500	1506.3	-4.0	-3.97
0.10	1500	1514.0	-4.0	-3.94
0.25	1500	1524.7	-4.0	-3.88

When the molecular ion concentration is greater than 10^2 cm^{-3} their currents also contribute appreciably to the determination of T_i. Thus it is important that the average mass of these ions should be known with some precision. A particular characteristic curve was analyzed in detail to determine the consequences of the assumed molecular mass on the derived value of T_i. The data were tape recorded in the 40 second mode-cycle on orbit 138 at 400 km altitude and at 17 degrees east geographic longitude and 50.6 degrees north geomagnetic latitude. Only one fourth of the data points recorded were used in the analysis. The results are shown qualitatively in Figure 10 where it is evident that the best fit is achieved by assuming the molecular ions have an average mass of 30 AMU. The quantitative parameters associated with these curves are summarized in Table II where by far the smallest σ is also associated with mass 30. This does not imply that only NO^+ was present, or indeed that it was the principal molecular ion. All that can be inferred is that the average molecular mass was closer to 30 AMU than to 28 AMU or 32 AMU.

Table II

Curve	Molecular Ion Mass (AMU)	Molecular Ion Conc. (cm^{-3})	Ion Temperature (°K)	σ (percent)
a	28	1.72×10^3	1331	9.64
b	29	1.27×10^3	1335	4.56
c	30	0.951×10^3	1380	1.41
d	31	0.723×10^3	1455	4.23
e	32	0.563×10^3	1537	7.06

The ion temperatures derived assuming 28 AMU and 32 AMU for the molecular ion mass differ by 3.6% and 11.4%, respectively, from the value obtained assuming 30 AMU. These differences are considerably larger than the scatter in the T_i data obtained in the absence of molecular ions, so it is clear that care needs to be taken in assigning a mass number to the heavy ions to avoid degrading the deduced values of T_i. The collector current values near the saturation region are relatively uninfluenced by the presence of the small concentration of molecular ions and an analysis of only the data points greater than one third the saturation current yields T_i = 1380°K, in very good agreement with the value obtained using mass 30. One might argue from this that T_i should be determined from only the upper portion of the data, and then one should separately deduce the molecular ion concentration. In the presence of horizontal fine structure in the ion concentration, however, this would be undesirable, as will be discussed later.

All the data shown in Figure 6 were analyzed with the assumption that the molecular ions were of mass 30 AMU. If it is discovered that this assumption about the molecular ion mass causes a serious degradation of the T_i values the difficulty can be eliminated for most of the data at some increase in the expense of data processing by the technique discussed. Another real check on the validity of the assumption of the molecular ion mass can be provided from the ion mass spectrometer on OGO VI, which should provide an independent measure of this quantity.

In the presence of fast electron fluxes the ion currents are measured from this background negative current (see Figure 2), which is assumed to be constant and independent of U. Of course as soon as U is low enough that an appreciable ion current is present the dependence of the negative current on U cannot be observed. On occasion, the angle of attack of the instrument is increased by purposely rotating the OPEP, and on these occasions the ion current begins at much lower values of U; even then, however, no change in the negative current is detected. Within the plasmasphere the negative currents are usually very small compared to the ion currents, and it is unlikely that any significant error in T_i is occasioned in this way. At high magnetic latitudes, and at high altitudes, this may not be true as large changes can occur in the negative currents, and the ion currents can become quite small. Under these conditions there are also usually large horizontal gradients in the ion concentrations and no attempt has been made to analyze the data.

A factor which could have an appreciable effect on the derived values of T_i is the unknown convection velocity of the plasma in the ionosphere. The quantity v that appears in (2) is the relative velocity of the vehicle with respect to the plasma, but in fact we use the vehicle velocity in the earth's frame of reference. Thus, any $\overline{E} \times \overline{B}$ drift of the plasma is unaccounted for in our analysis. When the analyzed ion currents can be attributed solely to O^+ the presence of $\overline{E} \times \overline{B}$ drift is not easily detected. Factors as large as 2 in T_i, with greatly different vehicle potentials, can be fitted to the data quite well when $\frac{\overline{E} \times \overline{B}}{B^2}$ is assumed as large 2 km/sec. Some upper limits on the assumed drift velocities can be set, i.e., the vehicle potential should not be positive, but even so, large uncertainties in T_i can arise.

When ion currents due to different mass ions are present these uncertainties are considerably reduced because an additional constraint is placed on the relationship between T_i and the vehicle potential, i.e., the characteristic energy width of the individual ion currents is proportional to $(\frac{m_i \, v \cos \theta}{\beta_i})$ and the energy displacement of the ion current curves is proportional to $(m_i \, v^2 \cos^2\theta)$. This restriction is exemplified in Figure 11 where the observed ion current characteristic (the same one shown in Figure 10) has been fit with different assumed values of v when appreciable molecular ions are present. The quantitative parameters associated with the curves in Figure 10 are summarized in Table III. In this case it appears that $\frac{\overline{E} \times \overline{B}}{B^2}$ drifts

normal to the sensor face as large as 200 m sec^{-1} would not be unnoticed, and even then the variance in the deduced value of T_i is not excessive. In fact the situation is somewhat worse than depicted because of the uncertainty in the molecular ion mass, which could probably be rationalized to give a good fit with either plus or minus 200 m sec^{-1}. In practice, however, there is an ion spectrometer on OGO VI that can remove any such ambiguities. At this early stage in the data analysis no such comparisons have been made.

Table III

Curve	Relative Velocity (km/sec)	Molecular Ion Conc. (cm^{-3})	Ion Temperature (°K)	σ (percent)
a	7.86	0.951×10^3	1380	1.41
b	7.66	1.18×10^3	1397	2.86
c	8.06	0.769×10^3	1376	3.18
d	6.00	7.00×10^3	2346	22.70
e	9.00	0.315×10^3	1393	11.70

It is not expected that large errors will accrue at low magnetic latitudes from the neglect of plasma drift, since the velocities are likely to be small within the plasmasphere. The corotation electric field gives rise to an east-west plasma drift of approximately 500 m sec^{-1} near the equator, but because of the nearly polar orbit only a small component of this velocity is normal to the sensor face. (The angle of

attack is offset approximately 4 degrees by the corotation, but this does not alter the normal velocity component used in the analysis.) At high magnetic latitudes plasma drift velocities may become quite large, and could introduce appreciable errors in the analysis. There is an experiment in the OGO VI that measures the component of the electric field responsible for the drift normal to the sensor face when the satellite is in a noon-midnight orbit plane, so it may be possible to quantitatively investigate the severity of this problem in the future.

Another parameter that could affect the error in T_i is the angle of attack. In principle the yaw and roll components of θ are held as close to zero as possible by the vehicle orientation system unless the OPEP is being purposely scanned or the vehicle turned to overcome windup along the solar paddle rotation axis. Ideally, the OPEP scan axis is kept pointing at the center of the earth. Since the orbit is slightly elliptical this would induce a finite pitch deviation in the OPEP angle of attack except at apogee and perigee. The amplitude of this effect is approximately 4 degrees for the actual orbit. The system-deduced value of θ is supplied in the regular data format so that the actual angle of attack can be allowed for. In practice θ appears never to exceed 5 degrees, except under the special conditions noted above, and even this maximum value would affect the derived T_i and n_i values by less than one percent if θ were assumed to be zero.

On one occasion when the OPEP was scanning (yaw rate $\sim$1.6 degrees sec^{-1}) in a rather uniform part of the ionosphere the ion temperature deduced at $\theta = 20°$ was calculated to be 2082°K when the proper value of θ was used and 1969°K when $\theta = 0°$ was assumed. The value of T_i deduced

when θ was actually near zero was 2065°K. Thus it appears that θ can usually be safely assumed to be zero during normal operations, and that reliable values of T_i can be recovered even when $\theta \leq 20°$, provided that θ is given.

Equation 2, from which the present results are obtained, is based on the so-called "planar approximation," i.e., it is assumed that the electric field associated with the vehicle potential is entirely normal to the sensor face. Thus all ions entering the trap will have energy $\varepsilon\psi$ added to their energy component normal to the trap face. The purpose of the wire screen surrounding the sensor head is to improve the validity of this approximation. The ratio of the plasma sheath length to the linear dimension of the equipotential surface surrounding the aperture is important in this regard. Quantitative evaluation of the appropriate correction is quite complicated, but some special cases have been considered theoretically (Knudsen, 1966; Whipple, 1969). The correctness of the approximation varies considerably over the orbit since the sheath length is proportional to $(\psi/\Sigma_i n_i)^{1/2}$, and both the vehicle potential and electron (ion) concentration exhibit large changes. Qualitatively, however, the effects of transverse electric fields in the sheath will be less important for ions with large mass than for those with small mass. This is true because the energy width, $(\frac{m_i V}{\beta_i})$, of the current-voltage characteristic curve is proportional to the square root of the ion mass, so that small spurious changes in ion energy will constitute a smaller error for heavier mass ions. In addition, the heavy ions receive smaller energy perturbations

from the transverse electric fields because of their larger inertia. In practice it has always been possible to achieve an excellent fit to (2) with the observed O^+ ion currents; this is not always the case for the H^+ and He^+ components. To date, no attempt has been made to correct for these effects in the analysis of the data, but qualitatively it is anticipated that they should increase the deduced values of T_i since the net effect is to increase the spread in the normal component of the ion energies.

The quality of the T_i data is adversely affected by gradients in n_i along the orbital path, but not so severely as might be expected. Consider the rather extreme case where n_i changes by a factor of two during the time the collector current increases by (say) a factor of 10^3. Since T_i varies as $\left(\frac{d\ \ell n\ J}{dU}\right)^{-2p}$ (where $1 \geq p(U) \geq 1/2$ for $f_i \leq 0$) this would result in an error of at most 20 percent in T_i. More likely changes in n_i, say 10 percent during the same time period, give rise to less than a 3 percent uncertainty in T_i. It would appear that quite reasonable values of T_i can be obtained in the presence of rather large concentration gradients, provided that the collector current can be measured over a sufficiently large dynamic range in a short enough time. In the presence of structure the 10 second mode-cycle time yields better T_i data than does the 40 second mode-cycle time.

Finally, a systematic error in the derived values of T_i is to be expected because the grids do not establish perfectly uniform potential surfaces. Not only are the ions defocussed by transverse electric fields near the grid wires, but also there are field depressions in the holes between grids that cause the effective sweep voltage to be smaller than that applied to the grid wires. (Hanson and McKibbin, 1961; Knudsen, 1966.) Both these effects would tend to increase the derived values of T_i. An attempt to evaluate these effects, which might raise T_i by several percent, is now being undertaken.

Comparisons are now being made with the various radar back scatter facilities, which also directly measure T_i. When these data have been processed the results should show whether or not the parameter we identify as T_i from the least squares fit actually corresponds to the real ion temperature.

Determination of n_i:

Laboratory tests have shown that the transmission factor, K, of the grid-stack is 0.410 $\pm$ .005 for ions in the appropriate energy range; this is essentially equal to the optical transmission factor. It is this value that is employed in (2) for data reduction. Other considerations, however, probably introduce larger uncertainties in the derived values of n_i, and again the problems are more severe for lighter ions. The fact that the aperture has a finite thickness (damn!) rather than a knife-edge introduces some fuzziness in the value of A, which depends on T_i, ψ, and m_i, but generally reduces the effective aperture area. Also, for large thermal ion velocities, the dispersion of the ions passing through the aperture can become appreciable and not all will strike the collector. Both of these effects tend to give an underestimate of the ion concentration. For O^+ and heavier ions the errors introduced by these effects under most conditions do not exceed a few percent, and even for lighter ions the increase in normal velocity due to the vehicle potential tends to minimize the effects. Still, corrections as large as 20 percent or more may be applicable for H^+ ions.

To some extent the focussing effect of the transverse electric fields in the sheath tends to offset the reduction in effective aperture area discussed above, particularly for large vehicle potentials. Quantitative evaluation of these various factors is quite complicated

and at present no attempt has been made to correct for them. About all that can be said at this stage is that the O^+ and molecular ion concentrations are unlikely to be in error by more than 10 percent, but a firm figure for the light ions is difficult to estimate.

Due to a failure in the solar paddle array (three weeks after launch) the vehicle potential became very large ($\sim$-20 volts) when the paddles were exposed to sunlight. At such large potentials the retarding potential is unable to bias the ambient ions from the collector, and even if this were possible it is unlikely that reliable T_i or n_i values could be obtained, though the duct mode still seems to be operable. Upon passage into eclipse the vehicle potential recovers quite rapidly, and some of these transition data have been examined. The analog data from one particular transition from high to low vehicle potential as the satellite passed into solar eclipse is shown in Figure 12. Since only analog data are available, the least squares analysis has not been applied so that mass composition data are not available. By inspection, however, it is estimated that there are approximately 2×10^4 light ions cm^{-3} and 10^4 O^+ ions cm^{-3}. Approximate values for vehicle potential at several points are also shown in the figure. The analog data to the left of those shown in Figure 12 were very similar to the first curve, and data recorded to the right were very similar to the last curve shown, although ψ did eventually decrease to approximately -3 volts. Figure 12 is a blowup of the trace where ψ decreased quite dramatically. The saturation ion current also decreased by nearly

20 percent during this mode-cycle and continued to do so until ψ became less than -5 volts. The total saturation current change was 33 percent, i.e., the ion concentration would have been overestimated in this instance by 50 percent, if sheath focussing were ignored. Such distortion effects should be larger for smaller ion concentrations, and smaller in the absence of light ions and at greater ion concentrations. A subsequent change in the solar paddle array occurred after several months such that the vehicle potential is much smaller in sunlight, though still of the order of -10 volts. It remains to be seen whether useful T_i values can be recovered from this data.

It should also be kept in mind that the above considerations neglect any effects due to $\overline{E} \times \overline{B}$ motion or to vertical streaming of the ions in the polar regions (Banks and Holzer, 1969). Electrodynamic drift into the trap face would cause an overestimate of n_i, whereas drift across the sensor axis would tend to cause ions entering the aperture to miss the collector. The latter effect will not be very important unless the drift speeds approach or exceed the satellite velocity.

Summary

Initial results obtained from the retarding potential analyser on OGO VI are very encouraging. It appears that reliable measurements of ion temperature are being obtained, but comparison with other techniques (e.g. radar backscatter) are needed to establish this

conclusively. The ion temperature is observed to be considerably higher in the winter hemisphere than in the summer hemisphere.

Because the collection efficiency for heavy (>14 AMU) ions is nearly constant and reasonably well understood, the ratio of the atomic (i.e. atomic oxygen and nitrogen) ion concentration to the molecular ion concentration can be determined with good precision, particularly if the molecular ion species are independently identified and their total concentration exceeds 100 ions per cubic centimeter.

The concentrations of H^+ and He^+ can also be determined when they are an appreciable fraction of the O^+ ion concentration, but with less confidence. The light ions can be detected at only a few percent of the O^+ concentration but they cannot be reliably separated unless their sum is greater than approximately ten percent of the O^+ concentration.

Electron fluxes with energies greater than approximately 10 ev are observed in the daytime, but with little directional information. Their source has not yet been identified but it seems likely that inside the plasmasphere they are due at least in part to ambient photoelectrons. Fine structure is observed in these fluxes poleward of approximately 60° magnetic latitude and the appearance of this structure may mark the boundary of the energetic trapped particle region, or possibly the plasma-pause, even at low altitudes.

The measurements have revealed considerable horizontal fine structure in ion concentration down to very small fractional amplitude changes. On occasion at low latitudes the ionosphere is observed to be

smooth to one part in a thousand over distances of several hundred kilometers. Over the polar regions, on the other hand, large horizontal concentration gradients exist. Fractional changes of a factor of two in a few kilometers are not uncommon; the amplitude of this structure appears to be greater at higher altitudes.

The usefulness of the measurements of the RPA will be greatly enhanced in the future when other ionospheric parameters also measured in OGO VI will be simultaneously available.

Acknowledgments:

The excellent engineering and technical support of J. Metrailer, L. Swaim, B. Holt, and W. Lane is gratefully acknowledged, as is the assistance of R. Cranley in the formulation of the least squares data fitting program. It is also a pleasure to recognize the most helpful efforts of many individuals on the OGO project team. This work was supported under NAS 5-9311.

References

Banks, P. M. and T. E. Holzer, The polar wind, J. Geophys. Res., 73, 6846, 1968.

Boyd, R. L. F. and W. J. Raitt, Positive ion temperatures above the F-layer maximum, Space Res., 5, 207, 1965.

Bowen, P. J., R. L. F. Boyd, W. J. Raitt, and A. P. Willmore, Ion composition of the upper F-region, Proc. Roy. Soc. A, 281, 504, 1964.

Donley, J. L., The thermal ion and electron trap experiments on the Explorer 31 satellite, Proc. IEEE, 57, 1061, 1969.

Donley, J. L., L. H. Brace, J. A. Findlay, J. H. Hoffman, G. L. Wrenn, Comparison of results of Explorer 31 direct measurements probes, Proc. IEEE, 57, 1078, 1969.

Dyson, P. L., Direct measurements of the size and amplitude of irregularities in the topside ionosphere, J. Geophys. Res., 74, 6291, 1969.

Hanson, W. B., and D. D. McKibbin, An ion-trap measurement of the ion concentration profile above the F2 peak, J. Geophys. Res., 66, 1667, 1961.

Hanson, W. B., D. D. McKibbin and G. W. Sharp, Some ionospheric measurements with a satellite-borne ion trap, J. Geophys. Res., 69, 2747, 1964.

Hanson, W. B., S. Sanatani, L. H. Brace and J. A. Findlay, Thermal structure of an Alouette 2 topside profile as deduced from rocket measurements, J. Geophys. Res., 74, 2229, 1969.

Harris, K. K., G. W. Sharp, and W. C. Knudsen, Ion temperature and relative ion composition measurements from a low-altitude polar-orbiting satellite, J. Geophys. Res., 72, 5939, 1967.

Harris, K. K., G. W. Sharp, and W. C. Knudsen, Gravity waves observed by ionospheric temperature measurements in the F region, J. Geophys. Res., 74, 197, 1969.

Johnson, C. Y., Ionospheric composition and density from 90 to 1200 km at solar minimum, J. Geophys. Res., 71, 330, 1966.

Knudsen, W. C., and G. W. Sharp, Evidence for temperature stratification in the E-region, J. Geophys. Res., 70, 143, 1965.

Knudsen, W. C., and G. W. Sharp, Ion temperature profile in the topside ionosphere, J. Geophys. Res., 71, 4099, 1966.

Knudsen, W. C., Evaluation and demonstration of the use of retarding potential analyzers for measuring several ionospheric quantities, J. Geophys. Res., 71, 4699, 1966.

Knudsen, W. C., and G. W. Sharp, Ion temperature measured around a dawn-dusk-auroral zone satellite orbit, J. Geophys. Res., 72, 1061, 1967.

Krassovsky, V. I., Exploration of the upper atmosphere with the help of the third Soviet sputnik, Proc. IRE, 47, 289, 1959.

McClure, J. P., Diurnal variation of neutral and charged particle temperatures in the equatorial F region, J. Geophys. Res., 74, 279, 1969.

Parks, C. G., Daytime flux of ionization from the ionosphere into the protonosphere, presented at the URSI Fall Meeting at Austin, Texas, 1969.

Patterson, T. N. L., Deduction of ionospheric parameters from retarding potential analyzers, J. Geophys. Res., 74, 4799, 1969.

Whipple, E. C., The ion-trap results in "Exploration of the upper atmosphere with the help of the third Soviet sputnik," NASA technical note No. D-665, 1961.

Whipple, E. C. and L. W. Parker, Theory of ion collection by traps and mass spectrometers with attractive apertures on moving charged spacecraft, presented at the A.G.U. Fall Meeting at San Francisco, Calif., 1969.

Wrenn, G. L., The langmuir plate and spherical ion probe experiments aboard Explorer 31, Proc. IEEE, 57, 1072, 1969.

Figure Captions

Fig. 1. Schematic cross-section of the sensor head, to scale. Cross-hatched sections are insulators. The place labeled C is the collector, and the bottom surface is the skin of the electronics box.

Fig. 2. A plot of raw data output, tape recorded at the 8 kbit telemetry rate, showing one complete cycle of both modes. Top trace is the electrometer output, the middle trace is from the switched words, and the lowest trace is a reconstructed retarding voltage sweep. Points A, B, C, and D are discussed in the text. Although the data were taken at the 8 kbit rate in the 40 second mode-cycle, only every fourth data point is shown so that the point density corresponds to that of the 10 second mode-cycle.

Fig. 3. Three illustrative traces of the difference amplifier output in the duct mode are shown. Tick marks at left divide vertical scale into three 5 volt sections. The percent indicator is applicable only to the lowest trace. The data were recorded in real time at the 64 kbit rate and plotted with a computer plotter. Negative changes in this signal correspond to positive gradients in ion concentration. The character of the traces is discussed in the text.

Fig. 4. Replot of raw data in Figure 2, showing ion current versus retarding potential. Solid points are the observed data and the solid line is the least squares fit of equation (2). Molecular ions and O^+ are present.

Fig. 5. Current-voltage characteristic curve taken when light ions (H^+ and He^+) and O^+ are present. The solid line is the theoretical equation (2) using the ionospheric parameter values shown in the figure. The data were tape recorded at the 8 kbit rate using the 40 second mode-cycle period.

Fig. 6. Plot of one nearly complete orbit of reduced data, showing ion composition, ion temperature, vehicle potential and electron flux as functions of magnetic latitude, altitude and geographic longitude. The areas designated "Polar Cap" refer to regions with large horizontal structure in ion concentration and electron flux. Their boundaries may mark the edges of the plasmapause, or perhaps of the energetic particle trapping region. The data is discussed at length in the text.

Fig. 7. Plot of photo-emission electron current to the collector from the elements inside the trap head due to solar UV as a function of the angle between the sun and the normal to the trap face.

Fig. 8. Plot of values of T_i obtained from consecutive sweeps versus magnetic latitude, showing the internal consistency of the derived parameter called ion temperature. The raw data were recorded in the ten second mode-cycle at the 8 kbit rate.

Fig. 9. Plot of the statistical-fit parameter σ (in percent) versus trial values of T_i for the data in Figure 10. Best values of ψ are also shown. The least squares program selected $T_i = 1380°K$ as the best fit.

Fig. 10. A composite plot of least squares fits to observed data assuming different mean molecular ion masses. Plots show best fit is obtained with a mean molecular mass of 30 AMU. See also Table II.

Fig. 11. Composite plot of least squares fits to the same data in Figure 10 assuming different relative velocities between the plasma and the sensor face. Pertinent parameters for the different curves are given in Table III.

Fig. 12. Plot of raw electrometer data output showing the effects of changing the vehicle potential from very high negative values to more normal values as the satellite moves into the darkness. The lower curve is a blowup of the trace during which the vehicle potential changed most drastically. The change in the saturation ion current during this sweep indicates that ions are focussed into the sensor aperture at large values of ψ. Data were recorded in real time in the 10 second mode-cycle.

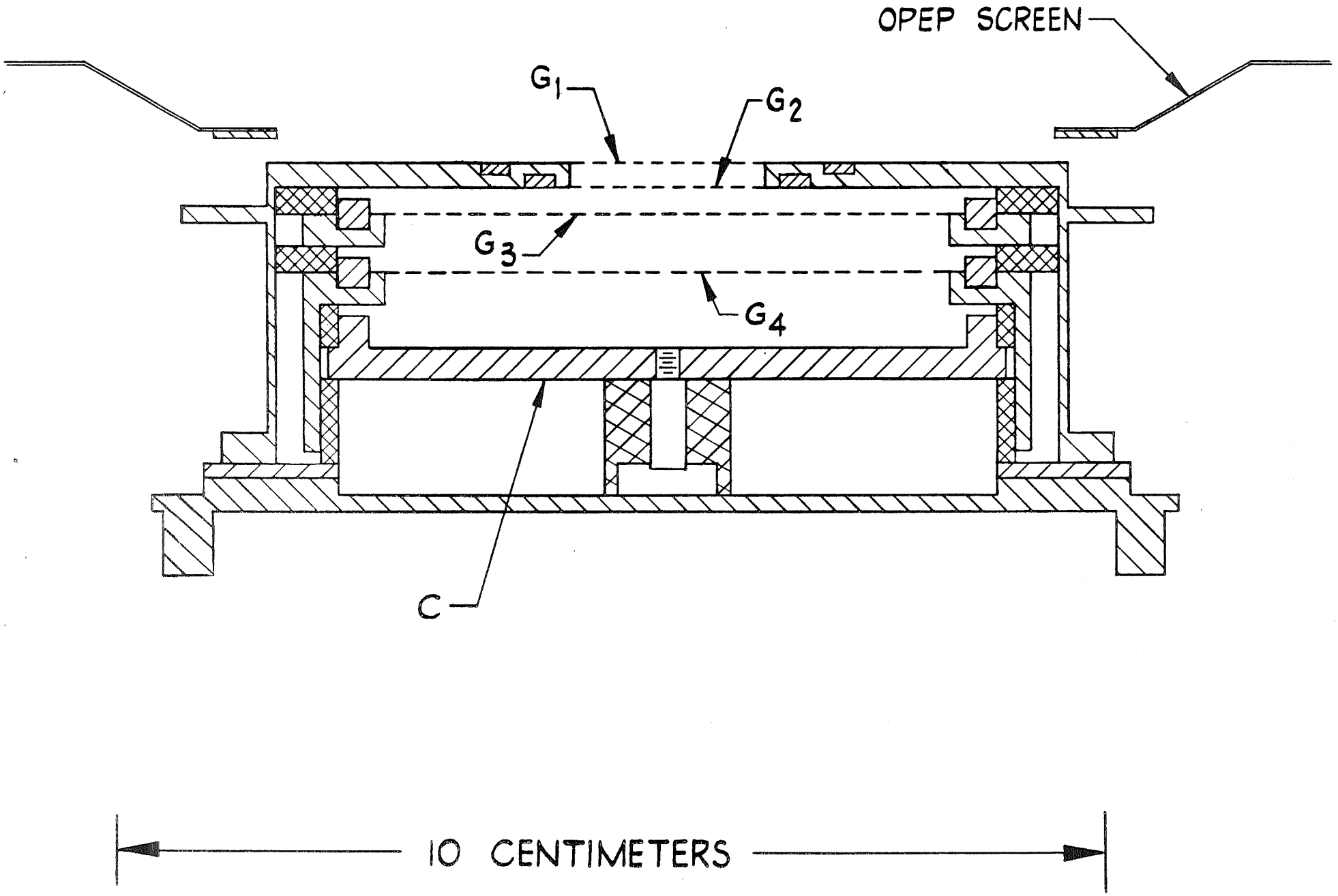

FIGURE 1

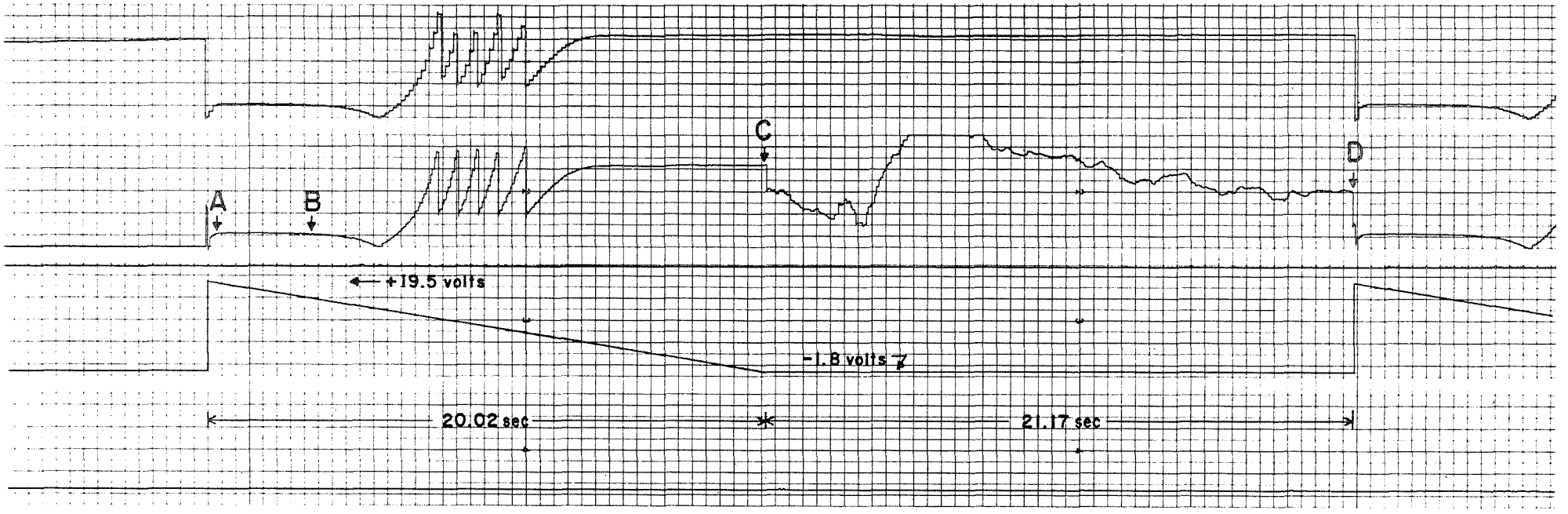

FIGURE 2

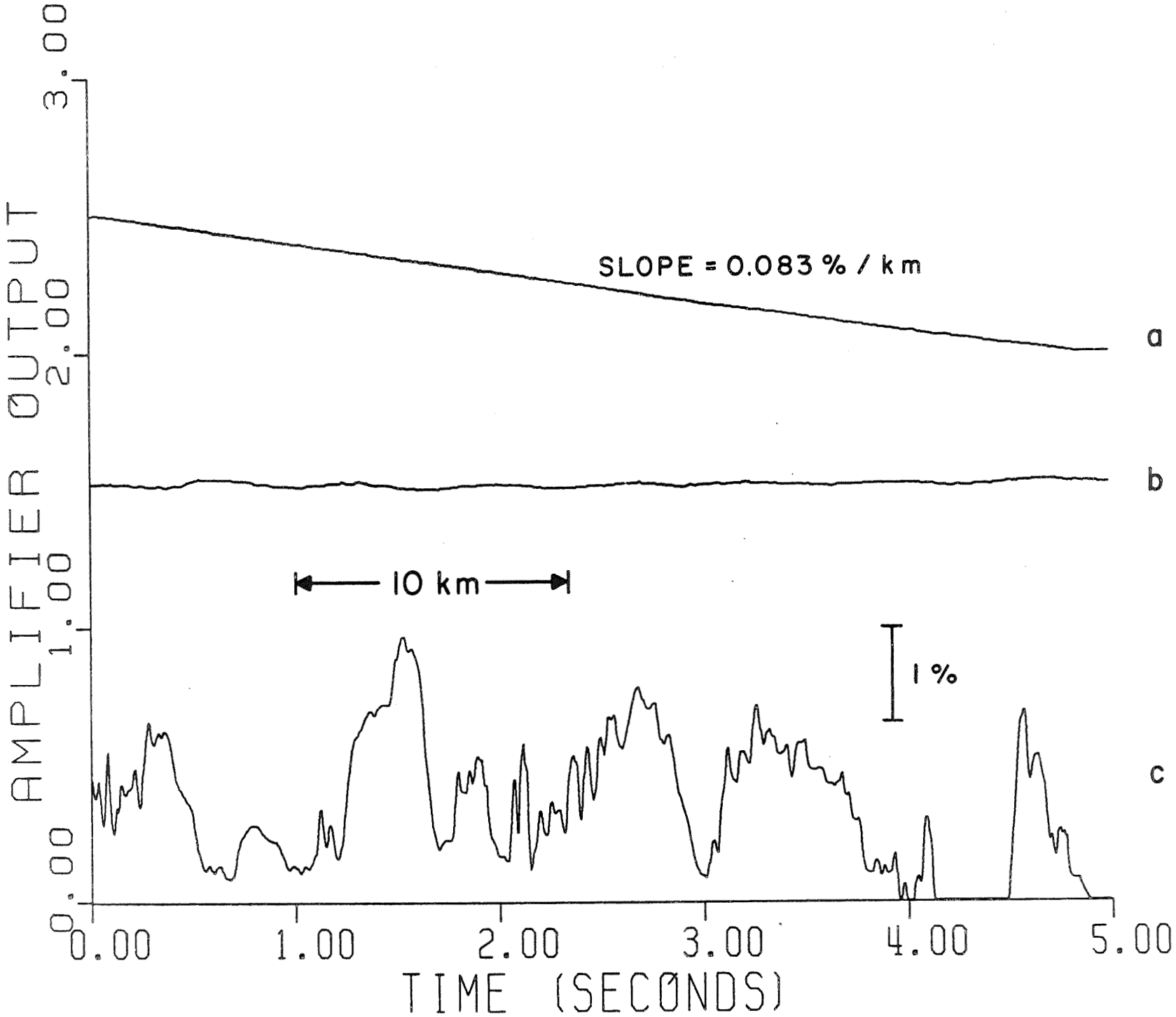
AMPLIFIER OUTPUT
3.00
2.00
1.00
0.00
SLOPE = 0.083 % / km
a
b
10 km
1 %
c
0.00
1.00
2.00
3.00
4.00
5.00
TIME (SECONDS)

FIGURE 3

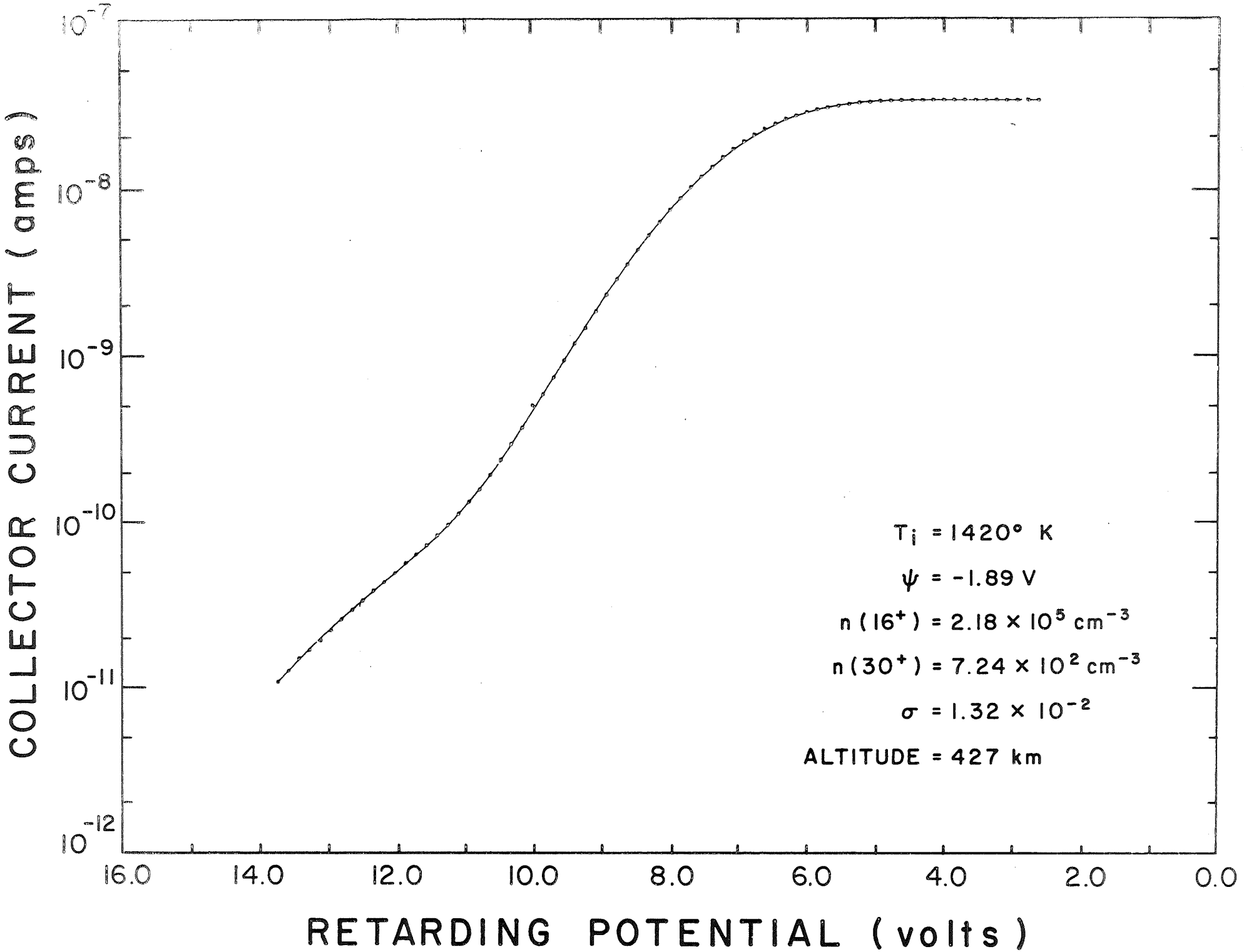
COLLECTOR CURRENT (amps)
10^{-7}
10^{-8}
10^{-9}
10^{-10}
10^{-11}
10^{-12}
16.0
14.0
12.0
10.0
8.0
6.0
4.0
2.0
0.0
RETARDING POTENTIAL (volts)
T_i = 1420° K
ψ = -1.89 V
n (16^+) = 2.18×10^5 cm^{-3}
n (30^+) = 7.24×10^2 cm^{-3}
σ = 1.32×10^{-2}
ALTITUDE = 427 km

FIGURE 4

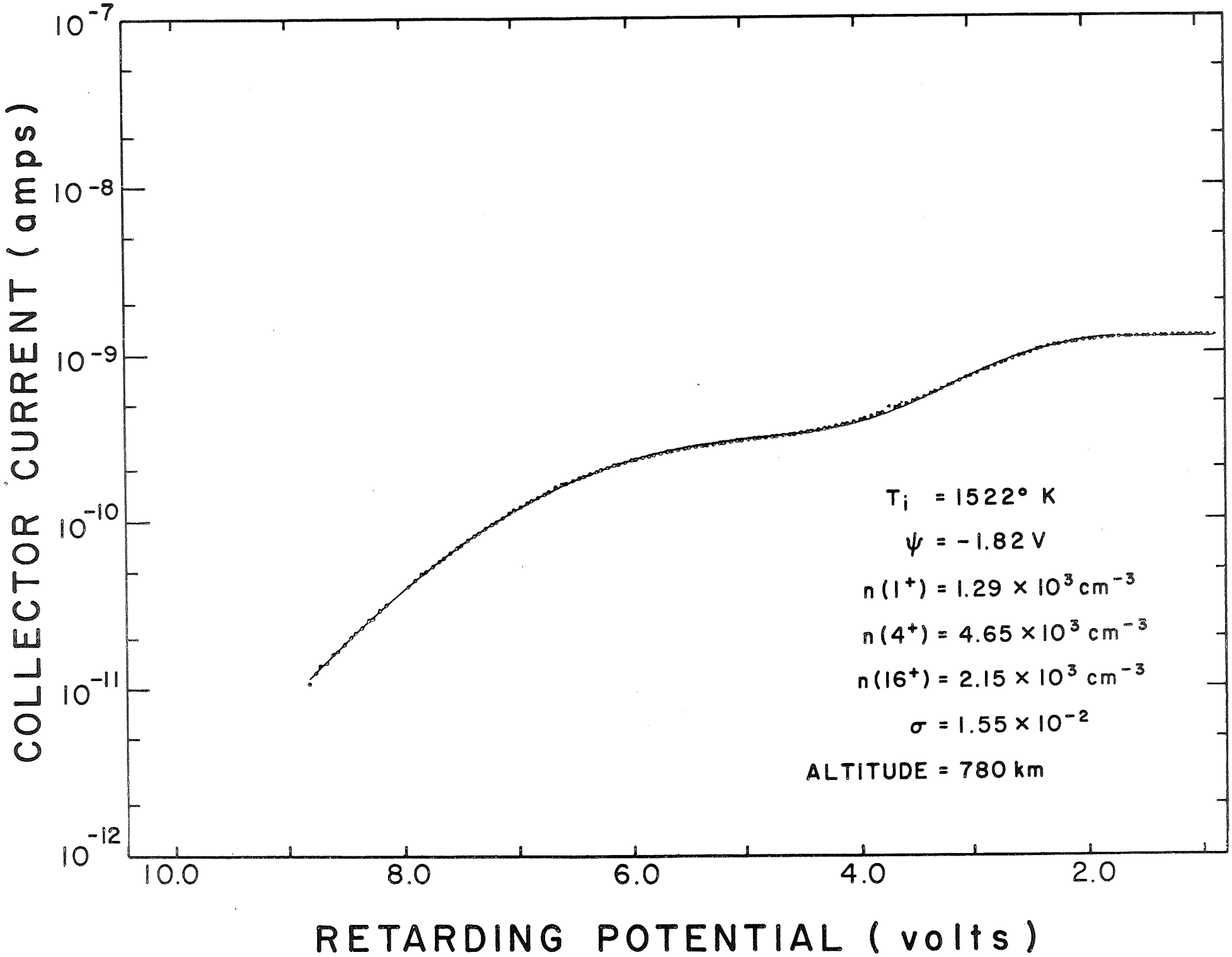
COLLECTOR CURRENT (amps)
10^{-7}
10^{-8}
10^{-9}
10^{-10}
10^{-11}
10^{-12}
10.0
8.0
6.0
4.0
2.0
RETARDING POTENTIAL (volts)
T_i = 1522° K
ψ = -1.82 V
$n(1^+) = 1.29 \times 10^3\ cm^{-3}$
$n(4^+) = 4.65 \times 10^3\ cm^{-3}$
$n(16^+) = 2.15 \times 10^3\ cm^{-3}$
$\sigma = 1.55 \times 10^{-2}$
ALTITUDE = 780 km

FIGURE 5

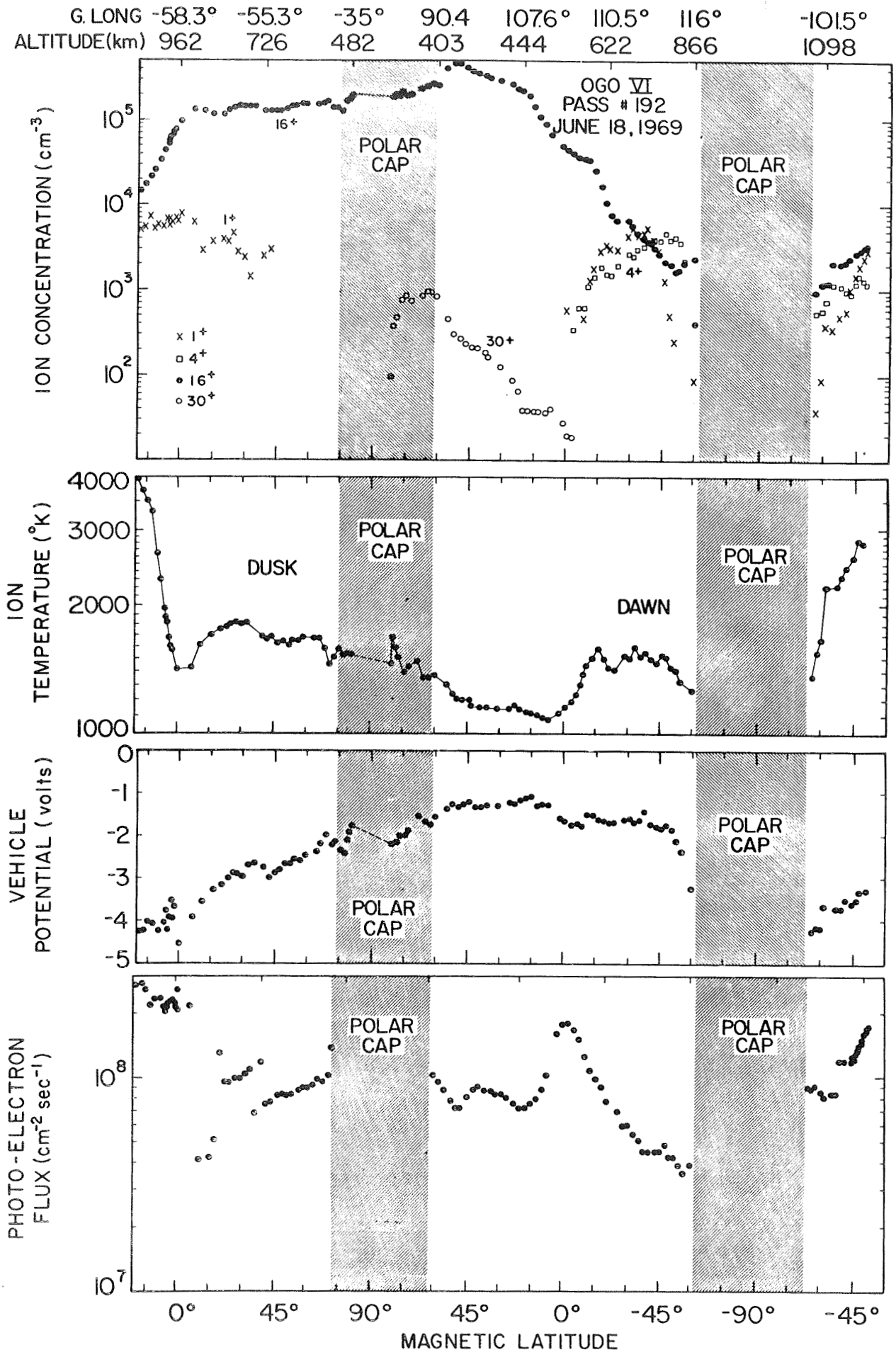
G. LONG -58.3° -55.3° -35° 90.4 107.6° 110.5° 116° -101.5°
ALTITUDE(km) 962 726 482 403 444 622 866 1098
OGO VI
PASS # 192
JUNE 18, 1969
ION CONCENTRATION (cm⁻³)
POLAR CAP
16+
1+
4+
30+
ION TEMPERATURE (°K)
DUSK
DAWN
VEHICLE POTENTIAL (volts)
PHOTO-ELECTRON FLUX (cm⁻² sec⁻¹)
0° 45° 90° 45° 0° -45° -90° -45°
MAGNETIC LATITUDE

FIGURE 6

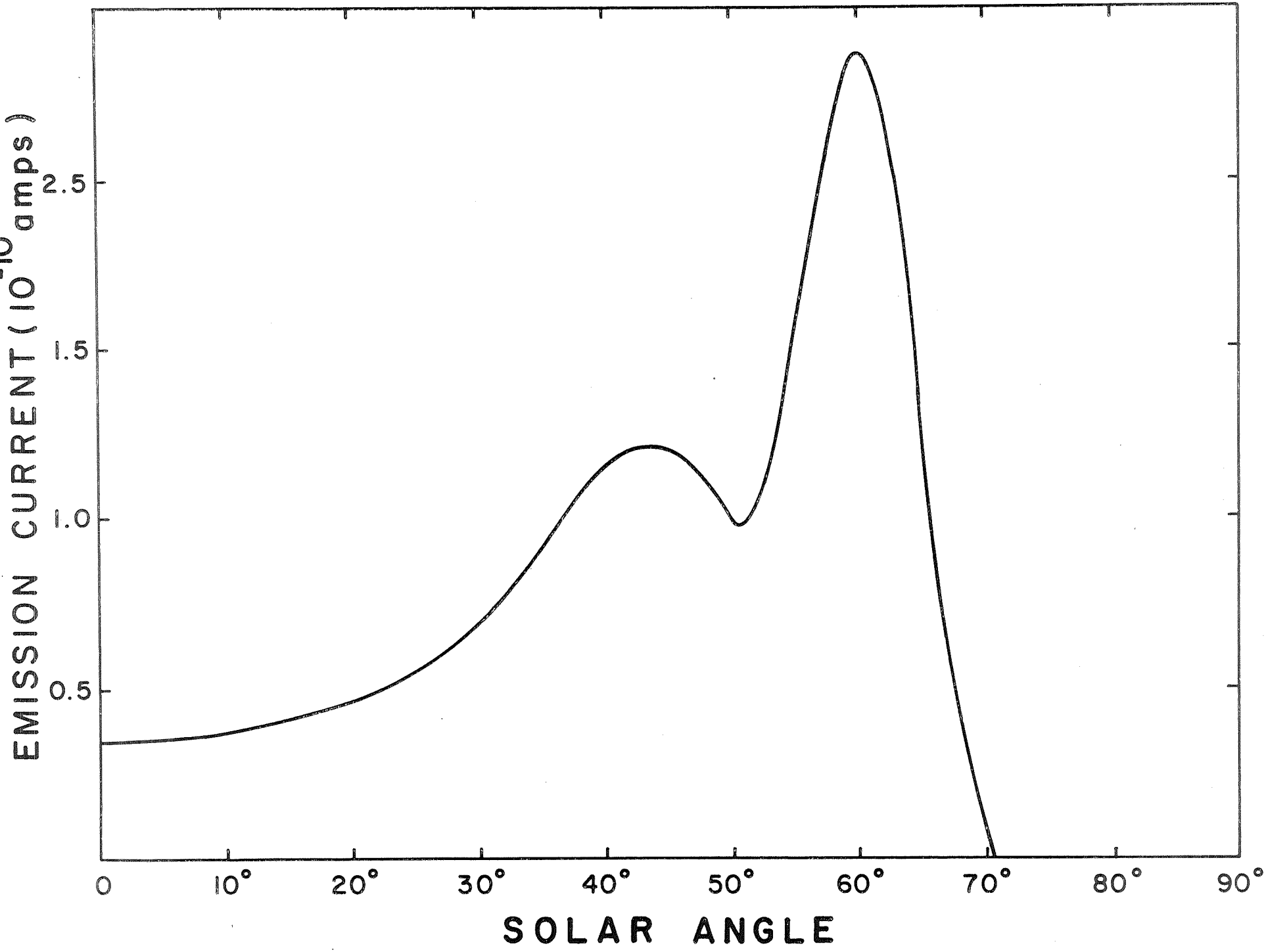
EMISSION CURRENT (10^{-10} amps)
2.5
1.5
1.0
0.5
0
10°
20°
30°
40°
50°
60°
70°
80°
90°
SOLAR ANGLE

FIGURE 7

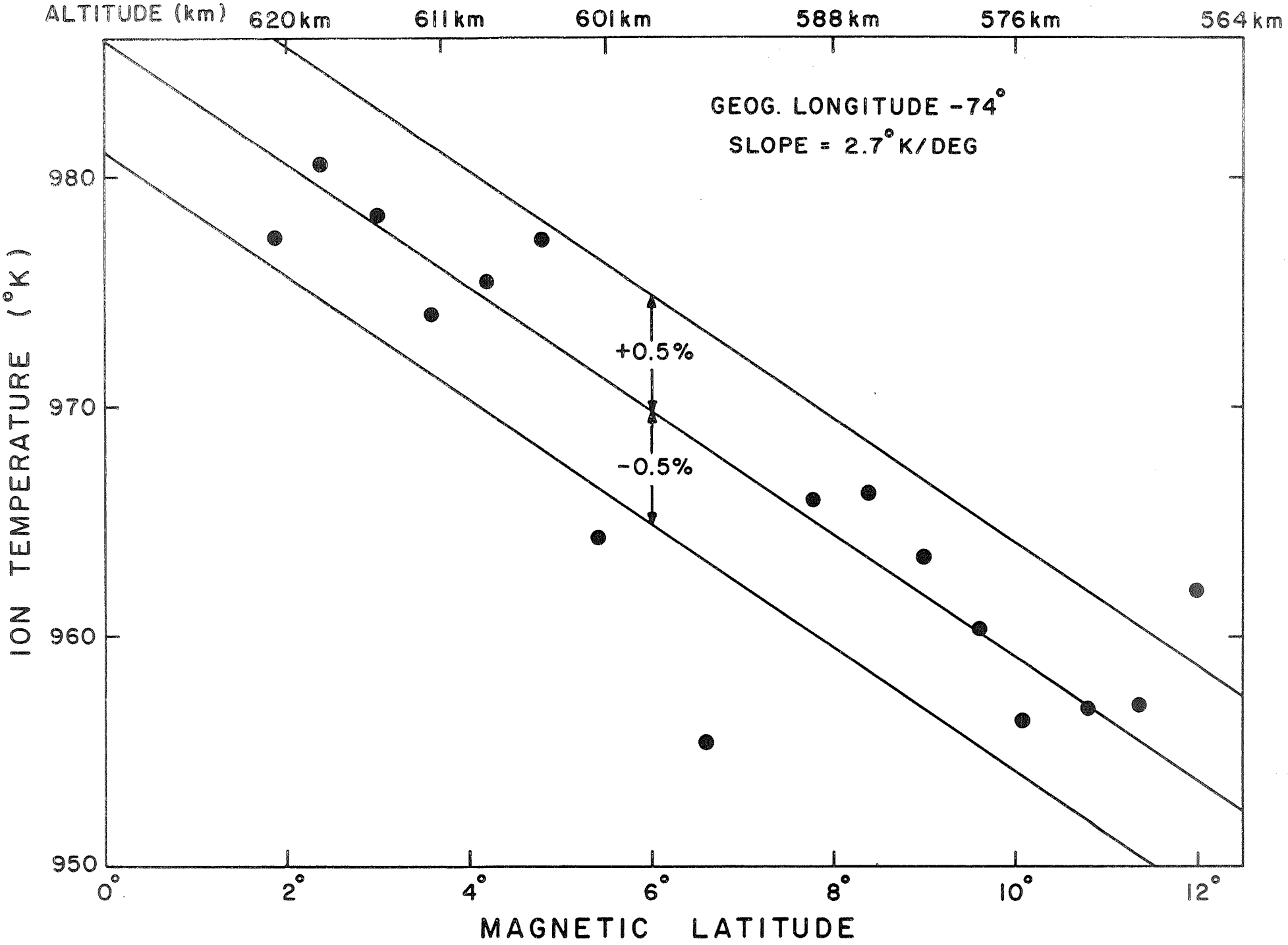
ALTITUDE (km)
620km
611km
601km
588km
576km
564km
GEOG. LONGITUDE -74°
SLOPE = 2.7°K/DEG
+0.5%
-0.5%
ION TEMPERATURE (°K)
980
970
960
950
0°
2°
4°
6°
8°
10°
12°
MAGNETIC LATITUDE

FIGURE 8

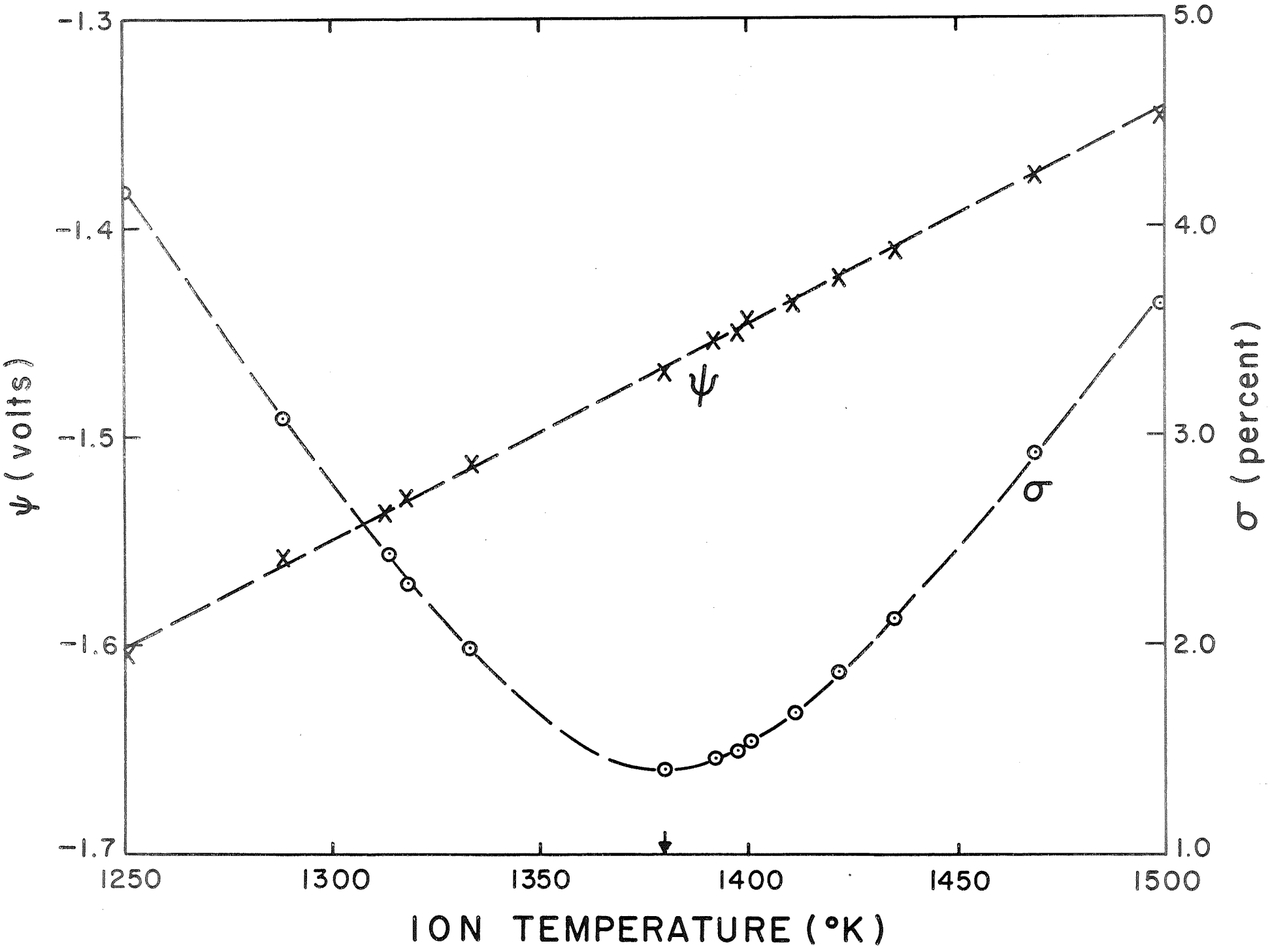
-1.3
-1.4
-1.5
-1.6
-1.7
ψ (volts)
5.0
4.0
3.0
2.0
1.0
σ (percent)
ψ
σ
1250
1300
1350
1400
1450
1500
ION TEMPERATURE (°K)

FIGURE 9

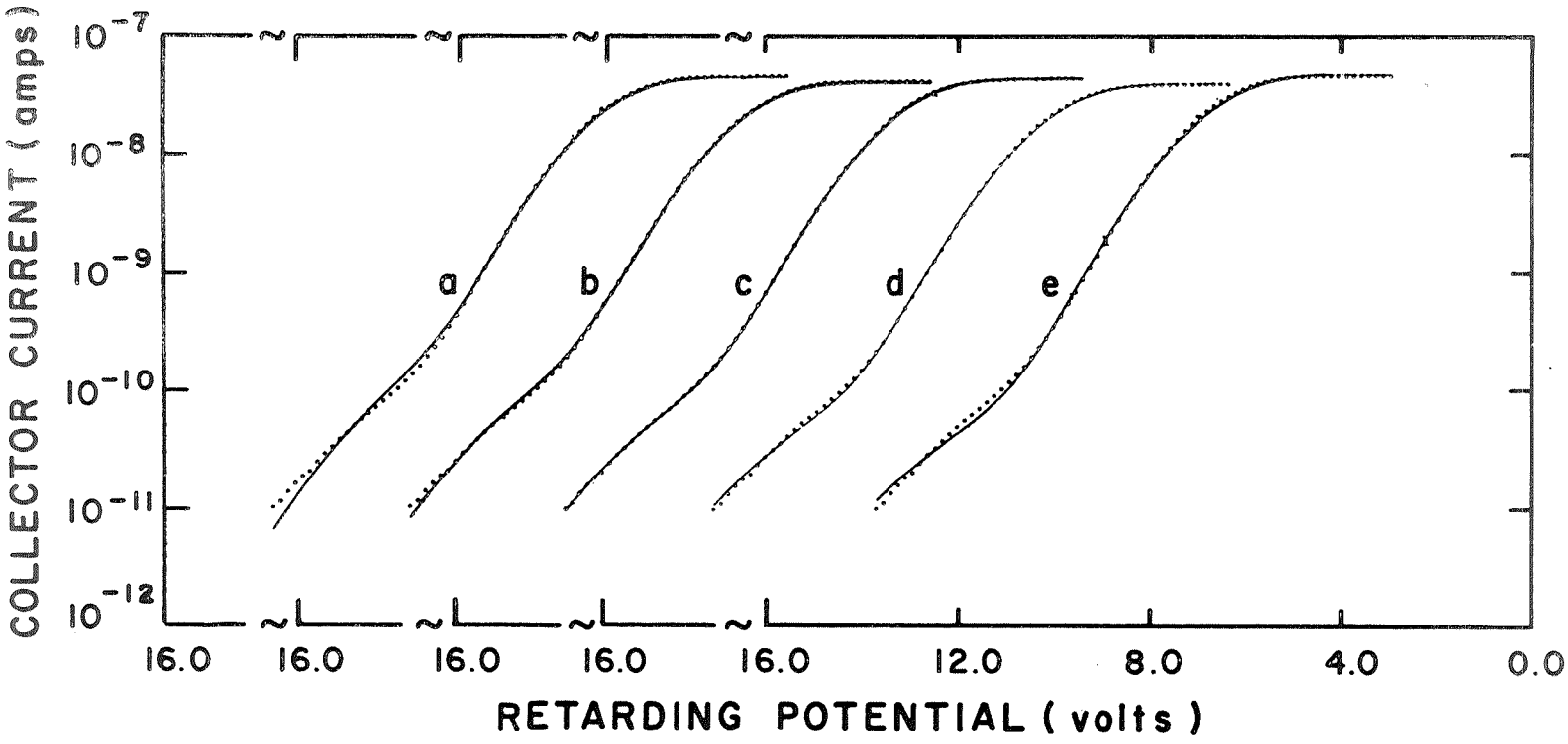
COLLECTOR CURRENT (amps)
10⁻⁷
10⁻⁸
10⁻⁹
10⁻¹⁰
10⁻¹¹
10⁻¹²
a
b
c
d
e
16.0
16.0
16.0
16.0
16.0
12.0
8.0
4.0
0.0
RETARDING POTENTIAL (volts)

FIGURE 10

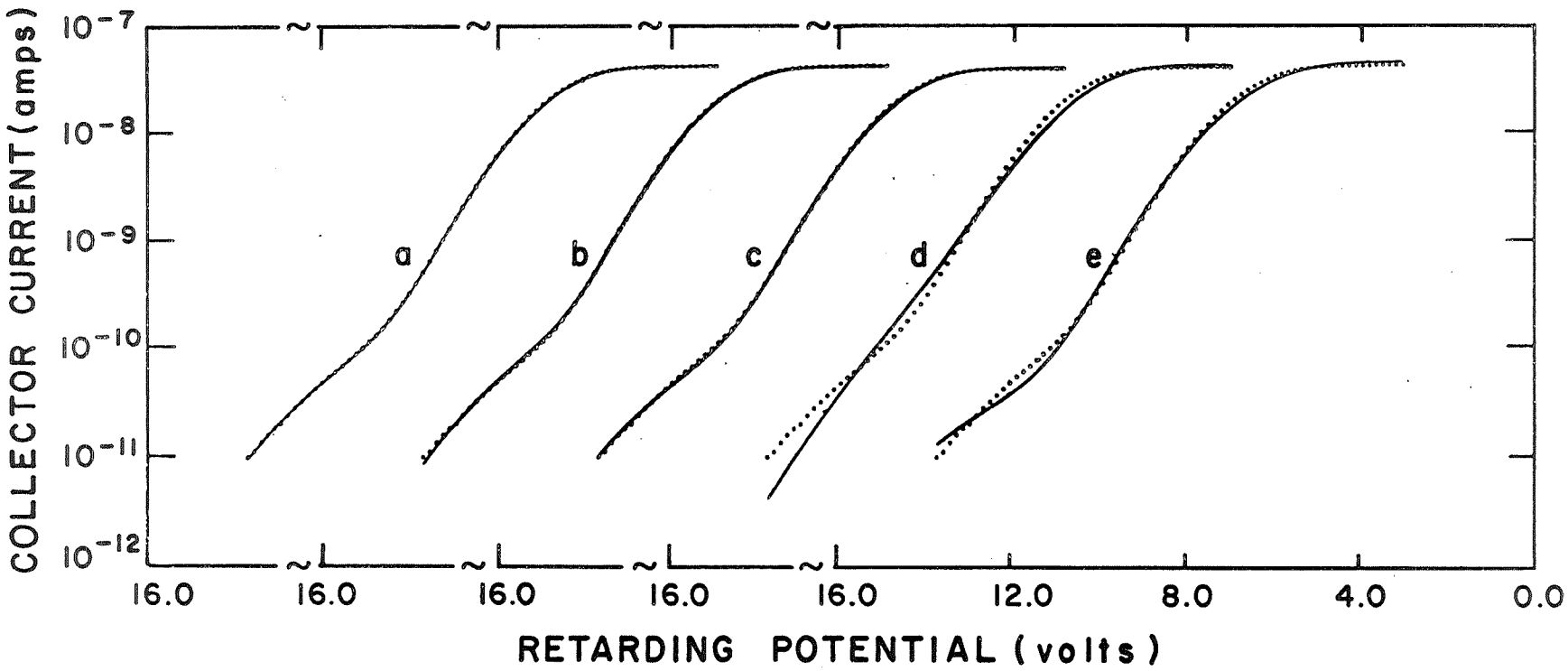
COLLECTOR CURRENT (amps)
10⁻⁷
10⁻⁸
10⁻⁹
10⁻¹⁰
10⁻¹¹
10⁻¹²
a
b
c
d
e
16.0
16.0
16.0
16.0
16.0
12.0
8.0
4.0
0.0
RETARDING POTENTIAL (volts)

FIGURE 11

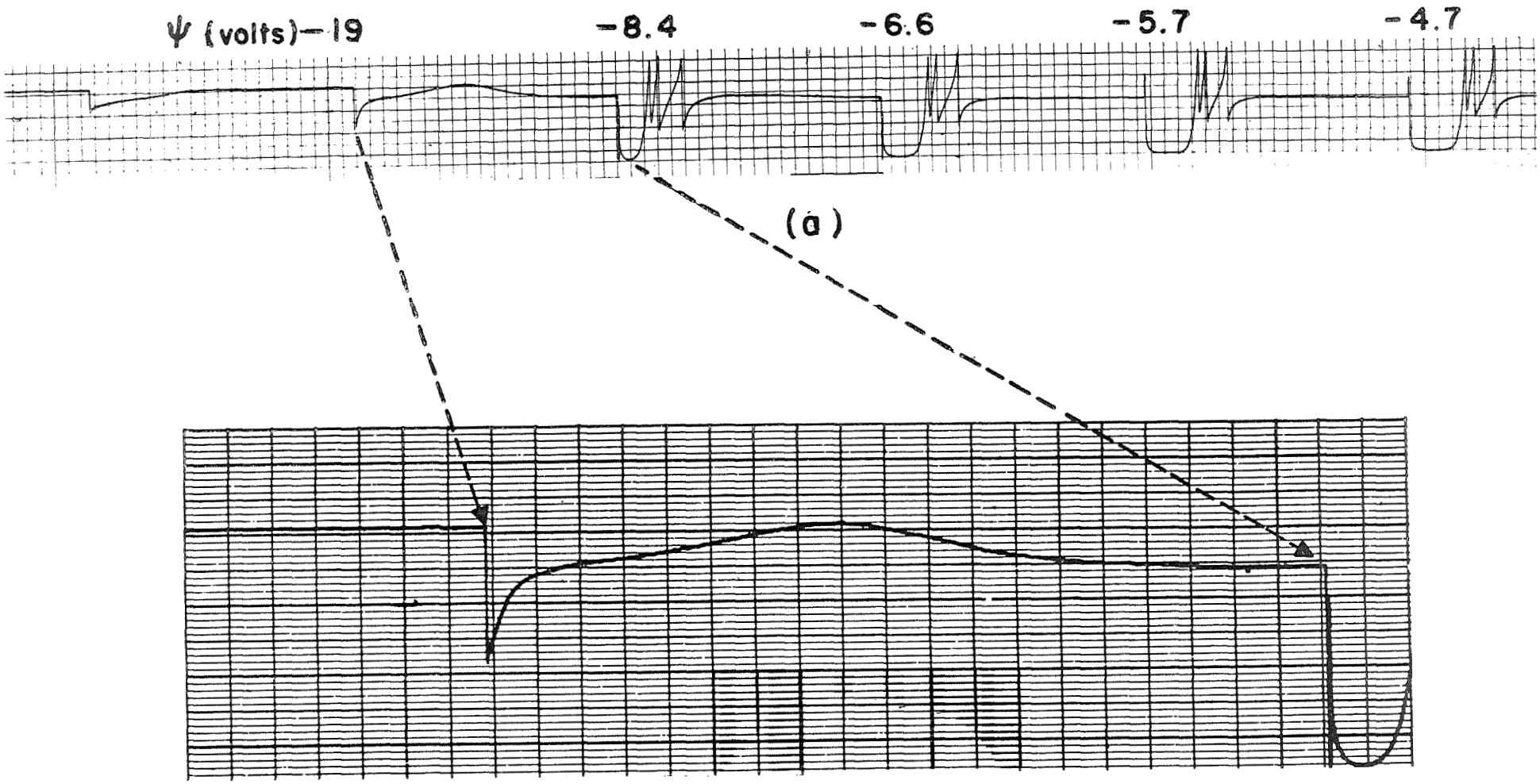
ψ (volts)—19
-8.4
-6.6
-5.7
-4.7
(a)